Better Understanding GPM Radiometer Measurements Using Ground-Based Radar

[1]Daniel Cecil, [2]Kenneth Leppert II, and [2]Themis Chronis

[1]NASA Marshall Space Flight Center, Huntsville, Alabama

[2]Earth System Science Center, University of Alabama in Huntsville, Huntsville, Alabama

1. Introduction

- Leppert and Cecil (2015) compared high-resolution airborne brightness temperatures (BTs) with a hydrometeor identification (HID) applied to ground-based, dual-polarimetric radar data using data from three days of intense convection during the Mid-latitude Continental Convective Clouds Experiment (MC3E) over Oklahoma in 2011.
- The BT data used in Leppert and Cecil (2015) was collected by the Advanced Microwave Precipitation Radiometer (AMPR) and Conically Scanning Microwave Imaging Radiometer (CoSMIR) at frequencies similar to those used by the Global Precipitation Measurement (GPM) Microwave Imager (GMI; 10−183 GHz [Hou et al. 2014]), and the radar data was obtained from the Vance, OK Weather Surveillance Radar – 1988 Doppler (WSR-88D) radar.
- Leppert and Cecil (2015) found that hail is associated with an ice-scattering signature at all frequencies examined, including 10.7 GHz, but frequencies ≤37.1 GHz appeared most useful for identifying hail.
- Graupel could be identified in the MC3E analysis by its strong scattering signature at higher frequencies (i.e., 165.5 GHz) and its relative lack of a scattering signature at frequencies ≤19.4 GHz.
- Another important result from the MC3E analysis of Leppert and Cecil (2015) is that the high frequency channels show potential for distinguishing particle types other than hail and graupel (e.g., wet snow, aggregates).
- The results shown here are a very preliminary expansion from the work of Leppert and Cecil (2015) by comparing GMI BTs with an HID applied to several WSR-88D radars.
- Specifically, this work is a proof-of-concept before advancing toward 2 primary objectives:
  1.) Build empirical relationships between GMI BTs and hydrometeor types derived from ground-based dual-polarization radar.
  2.) Build physical understanding of relationships between satellite measurements and hydrometeor types.

2. Data/Methodology

- Data: Passive microwave GMI BTs and GPM Ground Validation System Validation Network (VN) data (Schwaller and Morris 2011).
- The VN database consists of matched ground-based radar data (~70 WSR-88D radars mostly in the eastern half of the U.S.) and GPM satellite data from GPM overpasses that have at least 100 "Rain_Certain" pixels (from the GPM DPR 2A-Ku product) within at least 100 km of one of the ground-based radars. The VN dataset also includes an HID using an algorithm adapted from Dolan and Rutledge (2009) and used in Leppert and Cecil (2015).
- Data is used from March 2014 through April 2015.
- To minimize the effect of the signal from one hydrometeor species dominating the signal from other species and to better isolate the signal from each species separately, a subjective hierarchy of hydrometeor categories was applied. Each hydrometeor type was assigned a certain priority, and the type with the greatest priority was assigned to represent an entire vertical profile. The big drops category was given the highest priority followed by hail, high density graupel, low density graupel, rain, wet snow, aggregates, ice crystals (which were combined with vertically-oriented ice), and drizzle. The reasoning is that if hail, for example, is present anywhere in a column, its scattering will have a greater effect on the BT than any rain, ice crystals, etc., elsewhere in the column.

3. Example Cases

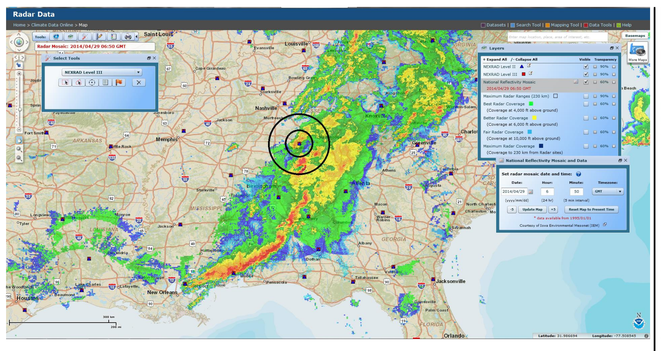

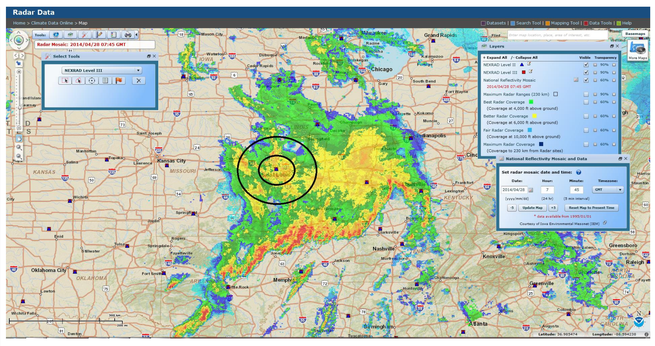

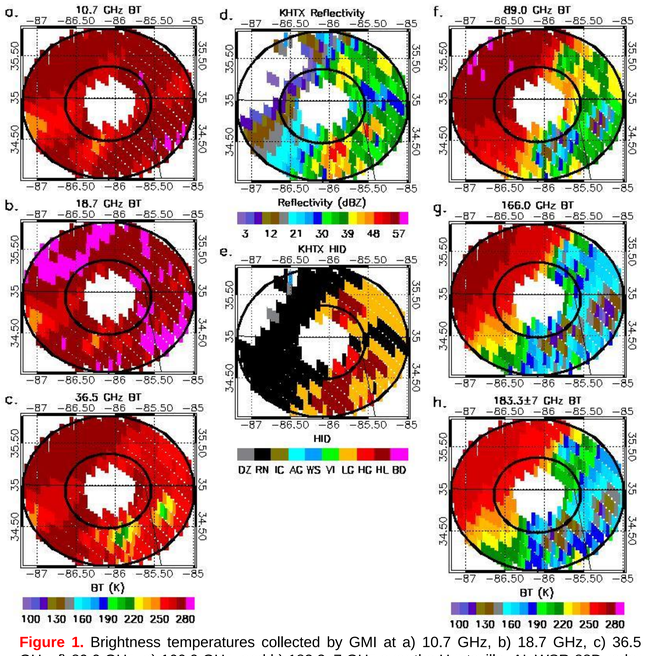

Figure 1. Brightness temperatures collected by GMI at a) 10.7 GHz, b) 18.7 GHz, c) 36.5 GHz, f) 89.0 GHz, g) 166.0 GHz, and h) 183.3±7 GHz over the Huntsville, AL WSR-88D radar (KHTX) on 29 April 2014 near 0650 UTC. The associated composite reflectivity and HID are shown in d) and e), respectively. The range rings are shown for 50 and 100 km. Note that data is excluded within 30 km of the radar to ensure adequate radar sampling through a deep layer, and the reflectivity data is averaged over the GMI resolution.

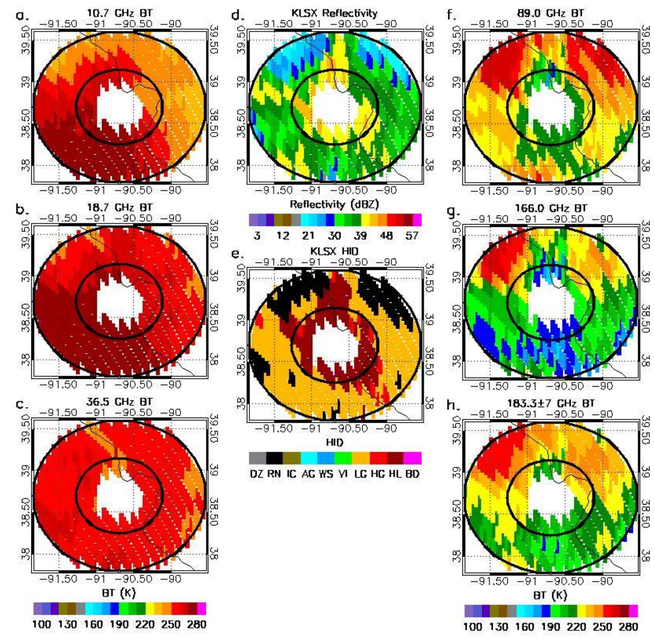

Figure 2. As in Fig. 1, but valid over the St. Louis, MO WSR-88D radar (KLSX) on 28 April 2014 near 0745 UTC.

- **Figure 1 shows a case with both convective and stratiform rain near Huntsville, AL. Two more intense "cells" are southeast of the radar (most apparent in the 36.5-GHz panel) with maximum reflectivity >48 dBZ and significant scattering in 36.5-GHz and higher frequency channels.**
- **As expected, hail and high density graupel are associated with these convective cores, while rain and low-density graupel are the dominant hydrometeor species in the weaker reflectivity regions elsewhere in Fig. 1.**
- **These convective cells exhibit a clear ice scattering signature at all frequencies ≥36.5 GHz with the lowest BTs observed at 89.0 and 166.0 GHz.**
- **The case depicted in Fig. 2 near St. Louis shows the trailing stratiform region of a mesoscale convective system with somewhat weaker reflectivity and ice scattering than observed in the most intense convection in Fig. 1.**
- **Nevertheless, hail and graupel are the predominant hydrometeor species shown in Fig. 2e. Note that even if one radar range gate in the matched GMI–radar volume is classified as hail, the application of the hydrometeor hierarchy will assign the entire volume to hail. Further investigation is required.**

4. Probability

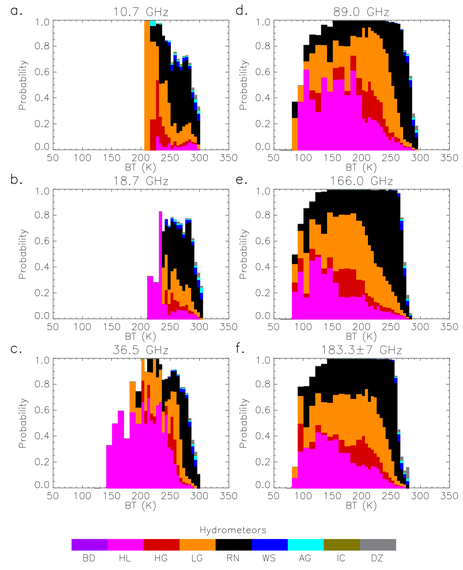

Figure 3. Probability of big drops (BD), hail (HL), high density graupel (HG), low density graupel (LG), rain (RN), wet snow (WS), aggregates (AG), ice crystals (IC), or drizzle (DZ) being the dominant hydrometeor type from the hierarchy as a function of a) 10.7-, b) 18.7-, c) 36.5-, d) 89.0-, e) 166.0-, and f) 183.3±7-GHz BT as measured by GMI. Data is taken from 268 GPM overpasses of WSR-88D radars in the southeastern U.S. during April–October 2014.

- **The low end of BTs shown in Fig. 3 are generally shifted to higher values than the low end of the BTs in Fig. 4 due to GMI having coarser horizontal resolution.**
- **Basic qualitative patterns are generally similar between Figs. 3 and 4.**
- **Figure 4 shows that hail, high density graupel, and associated big drops dominate at the lowest BTs for each frequency (Fig. 3 generally shows the same, except there are no identified big drops in the VN dataset).**
- **At warmer BTs in Fig. 4, wet snow and aggregates become most probable, especially at higher frequencies, while rain becomes most probable for warmer BTs in Fig. 3.**
- **These are preliminary results – much more investigation required!**

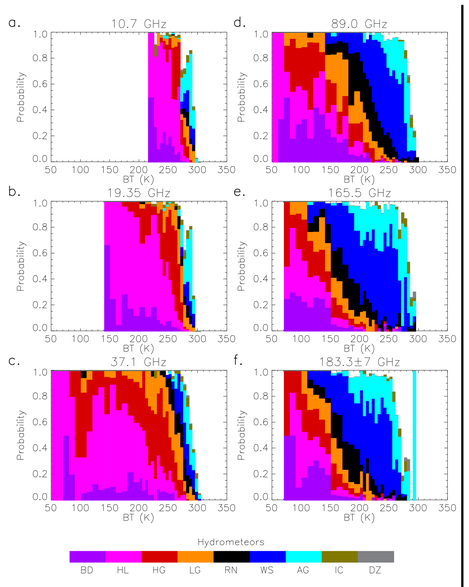

Figure 4. Probability of various hydrometeor species (same species as in Fig. 3) being the dominant species from the hierarchy as a function of a) 10.7-, b) 19.4-, c) 37.1-, d) 89.0-, e) 165.5-, and f) 183.3±7-GHz BT as measured by AMPR or CoSMIR on 22 April or 23−24 May 2011 over the KVNX radar. This figure is adapted from Leppert and Cecil (2015).

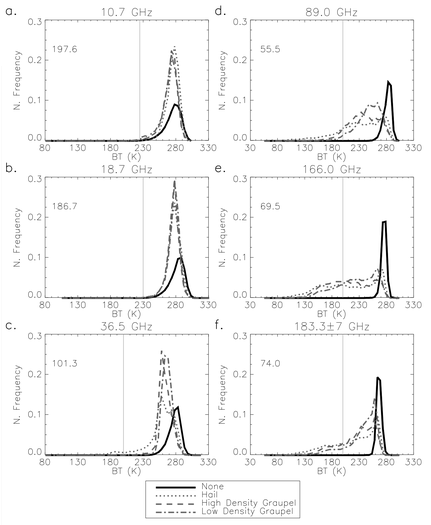

Figure 5. Brightness temperature probability distribution functions for vertical profiles that contain hail, high density graupel, low density graupel, and no hydrometeor types valid at a) 10.7, b) 18.7, c) 36.5, d) 89.0, e) 166.0, and f) 183.3±7GHz as measured by GMI. Data is taken **from 799 GPM overpasses** of WSR-88D radars over the eastern U.S. in the VN dataset during April–October 2014. The BT bin size is 10 (5) K to the left (right) of the vertical line in each panel, and the "*none*" frequency values have been scaled by 0.5 in order to limit the plottig range. The minimum BT measured at each frequency and associated with hydrometeors is indicated by the number in the top-left corner of each panel.

- **Figures 5 and 6 show the probability of measuring a certain BT given the presence of hail, graupel, etc., whereas Figs. 3 and 4 show the probability of finding a hydrometeor species given a particular BT.**
- **The PDFs are not noticably different for any of the precipitation-ice categories at frequencies ≥36.5 GHz in Fig. 5 from GMI. They are different in the higher-reolution airborne data (Fig. 6).**
- **At the highest frequencies, the distributions for hail and both graupel categories show greater separation from the distribution for the *none* category using MC3E data in Fig. 6 relative to what is observed in Fig. 5 with GMI data.**
- **Differences between Figs. 5 and 6 are not surprising given horizontal resolution differences of the BT data used for each figure.**
- **We have not worked with the VN data (at left) enough yet to have a fullunderstanding of all appropriate caveats**

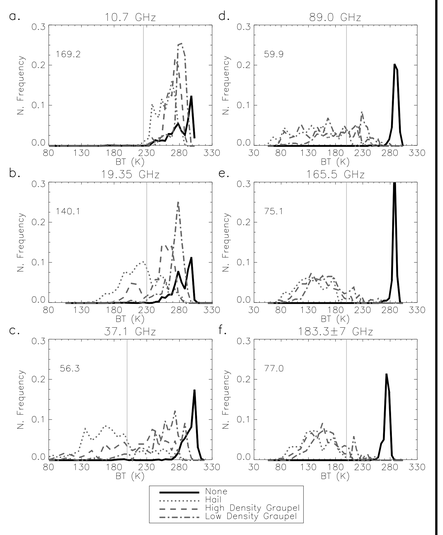

Figure 6. As in Fig. 5, except valid at a) 10.7, b) 19.4, c) 37.1, d) 89.0, e) 165.5, and f) 183.3±7GHz as measured by AMPR or CoSMIR on 22 April or 23−24 May 2011 over the KVNX radar. This figure is adapted from Leppert and Cecil (2015).

5. Conclusions

- **For the lowest BTs at all GMI frequencies, hail and graupel are most probable.**
- **Hydrometeor probabilities show the same general qualitative patterns using GMI data and higher-resolution MC3E data, but the lowest frequency GMI channels show less distinction between hydrometeor types (presumably due to beamfilling / footprint size).**
- **At higher frequencies, the distribution of BTs associated with profiles that contain hail or either graupel category shows greater separation from the distribution of BTs associated with profiles that contain no hydrometeors (i.e., a stronger ice-scattering signature) using the high-resolution data from Leppert and Cecil (2015) relative to the distributions using GMI BTs, as expected.**
- **Caveats: The High-Resolution results in Figure 6 are from a very limited sample of severe thunderstorm cases in MC3E. The Lower-resolution results in Figure 5 are from a larger sample that we have looked at much less carefully so far.**

6. References

- Dolan, B., and S. A. Rutledge, 2009: A theory-based hydrometeor identification algorithm for X-band polarimetric radars. *J. Atmos. Oceanic Technol.*, **26**, 2071–2088.
- Hou, A. Y., R. K. Kakar, S. Neeck, A. A. Azarbarzin, C. D. Kummerow, M. Kojima, R. Oki, K. Nakamura, and T. Iguchi, 2014: The Global Precipitation Measurement (GPM) mission. *Bull. Amer. Meteor. Soc.*, **95**, 701–722.
- Leppert, K. D., II, and D. J. Cecil, 2015: Signatures of hydrometeor species from airborne passive microwave data for frequencies 10–183 GHz. *J. Appl. Meteor. Climatol.*, **54**, 1313–1334.
- Schwaller, M. R., and K. R. Morris, 2011: A ground validation network for the Global Precipitation Measurement mission. *J. Atmos. Oceanic Technol.*, **28**, 301−319.

Acknowledgement:

We wish to acknowledge the NASA Precipitation Measurement Missions Science Team for funding this research, M. Schwaller and K. Morris for providing the VN data, and the Goddard Earth Sciences Data and Information Services Center for providing the GMI BT data.